THE JOURNAL OF BIOLOGICAL CHEMISTRY
Vol. 280, No. 6, Issue of February 11, pp. 5071–5081, 2005
Printed in U.S.A.

Crystal Structure of the Bovine Mitochondrial Elongation Factor Tu·Ts Complex*

Received for publication, October 18, 2004, and in revised form, November 12, 2004
Published, JBC Papers in Press, November 22, 2004, DOI 10.1074/jbc.M411782200

Mads Gravers Jeppesen‡§, Tomas Navratil§¶, Linda Lucy Spremulli§¶, and Jens Nyborg‡§‖

From the ‡Department of Molecular Biology, University of Aarhus, Gustav Wieds Vej 10 C, 8000 Aarhus C, Denmark and ¶Department of Chemistry, University of North Carolina, Chapel Hill, North Carolina 27599-3290

The three-dimensional structure of the bovine mitochondrial elongation factor (EF)-Tu·Ts complex (EF-Tu_{mt}·Ts_{mt}) has been determined to 2.2-Å resolution using the multi-wavelength anomalous dispersion experimental method. This complex provides the first insight into the structure of EF-Ts_{mt}. EF-Ts_{mt} is similar to *Escherichia coli* and *Thermus thermophilus* EF-Ts in the amino-terminal domain. However, the structure of EF-Ts_{mt} deviates considerably in the core domain with a five-stranded β-sheet forming a portion of subdomain N of the core. In *E. coli* EF-Ts, this region is composed of a three-stranded sheet. The coiled-coil domain of the *E. coli* EF-Ts is largely eroded in EF-Ts_{mt}, in which it consists of a large loop packed against subdomain C of the core. The conformation of bovine EF-Tu_{mt} in complex with EF-Ts_{mt} is distinct from its conformation in the EF-Tu_{mt}·GDP complex. When domain III of bovine EF-Tu_{mt}·GDP is superimposed on domain III of EF-Tu_{mt} in the EF-Tu_{mt}·Ts_{mt} complex, helix B from domain I is also almost superimposed. However, the rest of domain I is rotated relative to this helix toward domain II, which itself is rotated toward domain I relative to domain III. Extensive contacts are observed between the amino-terminal domain of EF-Ts_{mt} and domain I of EF-Tu_{mt}. Furthermore, the conserved TDFV sequence of EF-Ts_{mt} also contacts domain I with the side chain of Asp^{139} contacting helix B of EF-Tu_{mt} and inserting the side chain of Phe^{140} between helices B and C. The structure of the EF-Tu_{mt}·Ts_{mt} complex provides new insights into the nucleotide exchange mechanism and provides a framework for explaining much of the mutational data obtained for this complex.

Protein biosynthesis is the process by which the ribosome translates the sequence of nucleotides in a mRNA into the sequence of amino acids in a protein. During the cyclic elongation phase, the ribosome is assisted by elongation factors (EFs)[1] (1, 2). In prokaryotes, elongation factor EF-Tu promotes the binding of aminoacyl-tRNA (aa-tRNA) to the A-site of the mRNA-programmed ribosome in the form of the ternary complex aa-tRNA·EF-Tu·GTP (3). Upon cognate interaction between the codon of mRNA and the anticodon of aa-tRNA, GTP is hydrolyzed, and EF-Tu·GDP is released from the ribosome. The nucleotide exchange factor, EF-Ts, binds the EF-Tu·GDP complex mediating the release of the GDP and forms a stable EF-Tu·Ts complex (1). The high concentrations of GTP in the cell help dissociate EF-Ts leaving the active EF-Tu·GTP complex. EF-Tu·GTP binds another aa-tRNA, forming a new ternary complex, and the cycle is repeated.

Mitochondria contain a highly specialized protein biosynthetic machinery that is responsible for the synthesis of 13 polypeptides of the electron transport chain and the ATP synthase in the inner membrane (4). The mitochondrial translational system has a number of unique features including an altered genetic code, unusual protein-rich ribosomes, and tRNAs that lack many of the conserved residues found in canonical tRNAs (5–7). Despite these differences, mammalian mitochondria possess a translational elongation machinery with significant similarities to that of bacteria (8).

Mitochondrial EF-Tu (EF-Tu_{mt}) is highly conserved and is 55–60% identical to bacterial EF-Tu (9). The three-dimensional structure of the EF-Tu_{mt}·GDP complex has been determined at 1.94-Å resolution (10). The overall structure is similar to that observed in the *Escherichia coli* and *Thermus aquaticus* factors, but the nucleotide-binding domain (domain I) of EF-Tu_{mt} is in a different orientation relative to the rest of the structure compared with that observed in prokaryotic EF-Tu (11, 12). Furthermore, domain III is followed by a short 11-amino acid extension that forms one helical turn. This extension seems to be specific to the mitochondrial factors and has not been observed in any of the prokaryotic factors.

Bovine liver EF-Ts_{mt} is 338 amino acids in length. The amino terminus of the mature protein has been determined and indicates that removal of the 55-residue import signal leaves a mature protein of 283 amino acids (13). Bovine EF-Ts_{mt} is only 25–35% identical to its bacterial homologs, and primary sequence alignments are a challenge due to the limited conservation observed between the mitochondrial and prokaryotic factors.

Previous crystallographic studies have determined the structure of the EF-Tu·Ts complexes from *E. coli* and *Thermus thermophilus* (14, 15). The *E. coli* complex is a heterodimeric complex, whereas the *T. thermophilus* complex is heterotetrameric. In these complexes, EF-Ts makes extensive contacts with both domain I and domain III of EF-Tu. *E. coli* EF-Ts is organized into four structural modules (14): the amino-terminal domain (residues 1–54), the core domain (residues 55–179 and 229–263), the dimerization or coiled-coil domain (residues 180–228), and the carboxyl-terminal module (residues 264–282). The core domain can be further divided into subdomain N (residues 55–140) and subdomain C (residues 141–179 and 229–263). The amino-terminal domain, subdomain N, and the

* The costs of publication of this article were defrayed in part by the payment of page charges. This article must therefore be hereby marked "*advertisement*" in accordance with 18 U.S.C. Section 1734 solely to indicate this fact.

The atomic coordinates and structure factors (code 1XB2) have been deposited in the Protein Data Bank, Research Collaboratory for Structural Bioinformatics, Rutgers University, New Brunswick, NJ (http://www.rcsb.org/).

§ Supported by National Institutes of Health Grant GM32734-17.

‖ To whom correspondence should be addressed. Tel.: 45-89-42-52-57; Fax: 45-86-12-31-78; E-mail: jnb@imsb.au.dk.

[1] The abbreviations used are: EF, elongation factor; SeMet, seleno-L-methionine; P-loop, phosphate binding loop; DTT, dithiothreitol; PMSF, phenylmethylsulfonyl fluoride; MAD, multi-wavelength anomalous dispersion; PEG, polyethylene glycol.

carboxyl-terminal module interact with domain I of EF-Tu, whereas subdomain C interacts with domain III of EF-Tu. In the *T. thermophilus* $(EF\text{-}Tu\cdot Ts)_2$ complex, each EF-Tu moiety interacts with two EF-Ts subunits through a bipartite interface, which explains the need for an EF-Ts dimer in the nucleotide exchange reaction (15).

The mechanism of guanine nucleotide exchange in these factors is suggested to occur through a three-part mechanism. The interaction between EF-Tu and EF-Ts results in the disruption of the Mg^{2+} ion binding site, which leads to a reduced affinity of EF-Tu for guanine nucleotides. This process is induced by the intrusion of the side chains of Asp^{80} and Phe^{81} (*E. coli* numbering) from EF-Ts between helices B and C in domain I of EF-Tu. A peptide flip in the phosphate binding loop (P-loop) of EF-Tu destabilizes the binding of one β-phosphate oxygen of GDP. Finally, the movement of EF-Tu helix D affects the binding of the sugar and base of the bound nucleotide. The coordinated effects of this three-part mechanism lead to the release of GDP.

In the current study, we present the crystal structure of the bovine $EF\text{-}Tu_{mt}\cdot Ts_{mt}$ complex in the absence of any bound nucleotide at 2.2-Å resolution. The structure provides the first picture of the structure of the mitochondrial nucleotide exchange factor and provides insight into the mechanism of nucleotide exchange for this protein complex.

MATERIALS AND METHODS

Subcloning and Expression—The ligation independent cloning technique (Novagen) was used to remove the carboxyl-terminal His_6 tag on mitochondrial *Bos taurus* $EF\text{-}Tu_{mt}$ (9). The plasmid was purified by the miniprep procedure (Qiagen) and used as a template for PCR amplification using forward primer 5′-**GACGACGACAAGATG**TGATAAGAGGAGATATACAT*ATG*GCTGTGGAGGCCAAGAAGACC-3′ and reverse primer 5′-**GAGGAGAAGCCCGGT***TA*ACTCCACTTGATGTTCTTGTCCTCC-3′. The sequence required for ligation independent cloning is shown in bold in both primers, the ribosomal entry site is underlined, and the start codon is shown in italics in the forward primer. A stop codon in the reverse primer is also shown in italics.

The PCR product was inserted in the pET30 Ek/LIC vector according to the manufacturer's instructions (Novagen). The annealed vector and insert were transformed into NovaBlue heat competent *E. coli* cells (Novagen). A clone containing the insert, determined by restriction enzyme digestion, was sequenced using the BigDye Terminator v.3.1 kit (Applied Biosystems), verifying the removal of the His_6 tag. Isolated plasmids were then transformed into electrocompetent *E. coli* BL21(DE3) cells for expression.

Purification of Untagged SeMet Substituted EF-Tu$_{mt}$—The SeMet media consist of 1 μg/ml of vitamins (riboflavin, niacinamide, pyridoxine monohydrochloride, and thiamine), 40 μg/ml of all amino acids except methionine, 40 μg/ml SeMet, 25 μg/ml $FeSO_4$, 0.4% (w/v) glucose, 2 mM $MgSO_4$, 2 mg/ml NH_4Cl, 6 mg/ml KH_2PO_4, and 25.6 mg/ml $Na_2HPO_4\cdot 7H_2O$. All amino acids, vitamins, and glucose were filter sterilized through a 0.2-μm filter (Sartorius). The water and a 10× $(NH_4Cl/KH_2PO_4/Na_2HPO_4\cdot 7H_2O)$ solution were filtered through a 0.22-μm filter (Millipore) and autoclaved before mixing (16).

Instead of transforming the SeMet autotroph *E. coli* strain Bl21(DE3)834, the normal BL21(DE3) strain was used for the expression of SeMet protein. SeMet media (50 ml) containing kanamycin at 25 μg/ml were inoculated with *E. coli* BL21(DE3) cells expressing untagged *B. taurus* $EF\text{-}Tu_{mt}$ and grown overnight at 37 °C. The cells were spun down and resuspended in 100 ml of fresh SeMet media, which were used to inoculate 1850 ml of SeMet media containing 25 μg/ml kanamycin. The cells grew at 37 °C to an A_{600} of 1.2–1.5, at which protein expression was induced with 0.25 mM isopropyl β-D-thiogalactopyranoside for 8 h (also at 37 °C). The cells were collected by centrifugation and resuspended in 2 ml of lysis buffer (40 mM KCl, 50 mM Hepes-NaOH, pH 7.5, 10% (v/v) glycerol, 15 μM GDP, 10 mM $MgCl_2$, 3 mM DTT, 0.5 mM phenylmethylsulfonyl fluoride (PMSF), and 0.5 mM NaN_3) per gram of wet cells and frozen at −20 °C. The cells were ruptured in an EmulsiFlex-05 high pressure cell homogenizer (Avestin) at ~15,000 p.s.i. and ultracentrifuged at 50,000 rpm for 75 min at 4 °C. The supernatant was filtered through a 0.45-μm filter (Sartorius) and loaded on a 120-ml Source 30Q column (Amersham Biosciences) equilibrated in lysis buffer. The protein was eluted with a 400-ml linear gradient of 0–25% S30Q-B buffer (lysis buffer containing 1 M KCl). The flow rate was 2 ml/min, and 5-ml fractions were collected. Fractions containing the protein of interest as determined by SDS-PAGE were pooled. The pooled protein was precipitated overnight with ~70% $(NH_4)_2SO_4$ and collected by low-speed centrifugation. The pelleted protein was resuspended in buffer HIC A (1.5 M $(NH_4)_2SO_4$, 50 mM Hepes-NaOH, pH 7.5, 10% glycerol, 5 mM $MgCl_2$, 15 μM GDP, and 1 mM DTT). The pH of the buffer was adjusted to 7.5. A portion of the protein was loaded on a 1-ml ISO Resource column (Amersham Biosciences) equilibrated in HIC A. The purity of EF-Tu in the flow-through fractions was close to 95% as assessed by SDS-PAGE, and no further purification was necessary. Fractions containing the protein were pooled and concentrated in a YM-30 Centricon tube (Amicon), glycerol was added to a final concentration of 20%, and the sample was frozen in liquid nitrogen and stored at −80 °C.

Purification of EF-Ts$_{mt}$—A single colony of cells expressing carboxyl-terminally His_6-tagged $EF\text{-}Ts_{mt}$ (13) was grown in 4 liters of LB media containing 25 μg/ml kanamycin at 37 °C while shaking until an A_{600} of 0.7–0.9 was reached. Protein expression was induced with 0.25 mM isopropyl β-D-thiogalactopyranoside for 3.5 h (also at 37 °C), and the cells were harvested by centrifugation at 4 °C. The wet cells were resuspended in $EF\text{-}Ts_{mt}$ lysis buffer (150 mM KCl, 50 mM Tris-HCl, pH 7.6, 10% glycerol, 2 mM $MgCl_2$, 15 μM GDP, 2 mM β-mercaptoethanol, and 0.5 mM PMSF) to a total of 50 ml and stored at −20 °C. The thawed cells were broken using the EmulsiFlex-05 high pressure cell homogenizer (Avestin). The lysed cells were subjected to ultracentrifugation at 50,000 rpm for 75 min at 4 °C. The pH of the supernatant was adjusted to ~8 with Tris-HCl and applied to a nickel-nitrilotriacetic acid column (Amersham Biosciences) equilibrated in $EF\text{-}Ts_{mt}$ lysis buffer. The column was washed with NH_4Cl wash buffer (1 M NH_4Cl, 50 mM Tris-HCl, pH 7.6, 5 mM $MgCl_2$, 10% glycerol, 15 μM GDP, 2 mM β-mercaptoethanol, and 0.5 mM PMSF) in order to minimize the fraction of $EF\text{-}Ts_{mt}$ that would otherwise be associated with the *E. coli* EF-Tu. The *E. coli* EF-Tu·$EF\text{-}Ts_{mt}$ complex was eluted with $EF\text{-}Ts_{mt}$ elution buffer (40 mM KCl, 50 mM Tris-HCl, pH 7.6, 10% glycerol, 2 mM $MgCl_2$, 15 μM GDP, 2 mM β-mercaptoethanol, and 0.5 mM PMSF) containing 40 mM imidazole-HCl, pH 8. The remainder of the protein bound to the column was eluted with $EF\text{-}Ts_{mt}$ elution buffer containing 250 mM imidazole-HCl, pH 8. This latter portion contains mainly $EF\text{-}Ts_{mt}$.

The eluted portion containing $EF\text{-}Ts_{mt}$ was clarified in a tabletop centrifuge at 15,000 rpm for 10 min at 4 °C before being loaded on a 10-ml Source Q column (Amersham Biosciences) equilibrated in $EF\text{-}Ts_{mt}$ Source Q Buffer A (40 mM KCl, 50 mM Tris-HCl, pH 7.6, 2 mM $MgCl_2$, 10% glycerol, 1 mM DTT, and 0.5 mM PMSF). The protein was eluted with a gradient from 0% to 50% Source Q Buffer B (Source Q Buffer A containing 0.5 M KCl). Fractions containing $EF\text{-}Ts_{mt}$ were pooled and concentrated in a YM-10 Centricon tube (Amicon). Glycerol was added to the concentrated protein to a final concentration of 20%, and the sample was stored at −80 °C.

Crystallization—Samples containing untagged SeMet substituted $EF\text{-}Tu_{mt}$ and carboxyl-terminally His_6-tagged $EF\text{-}Ts_{mt}$ were thawed on ice. The concentrations of both proteins were determined by the Bradford method (17) using bovine serum albumin as the standard. The two proteins (~5 mg of each) were mixed in a molar ratio of 1:1.3 $EF\text{-}Tu_{mt}\cdot Ts_{mt}$ and left on ice for approximately 1 h. The mixture was then dialyzed against 1.5 liters of 20 mM Hepes-NaOH, pH 7.5, 75 mM KCl, 5 mM EDTA-NaOH, pH 8, 1 mM DTT, and 0.5 mM NaN_3 overnight and dialyzed the next morning for 2 h against a new 0.5 liter of the same buffer. The 1.5-ml sample was then clarified in a tabletop centrifuge at 15,000 rpm for 10 min at 4 °C and applied to a 120-ml (2 × 60-cm) Sepharose S100 HR gel filtration column (Amersham Biosciences) equilibrated in buffer GF (20 mM Hepes-NaOH, pH 7.5, 75 mM KCl, 1 mM DTT, and 0.5 mM NaN_3). Fractions containing the complex were concentrated in a YM-50 Centricon tube (Amicon) to ~6.5 mg/ml, and crystallization trials were set up.

The SeMet substituted protein complex was crystallized by the sitting drop vapor diffusion technique by mixing 1 μl of protein solution with 1 μl of reservoir solution (14–18% PEG 8k, 100 mM Tris-HCl, pH 7.6, 200 mM trisodium citrate·$2H_2O$, 2 mM DTT, and 1 mM NaN_3) followed by equilibration against the reservoir at 6 °C. One day after setup, the drop was streak-seeded using native crystals. The crystals appeared within 1 day after this and grew to a maximum of 500 × 200 × 100 μm in 2–3 weeks.

Data Collection and Processing—A crystal of SeMet substituted protein was transferred to stabilization buffer (20% (w/v) PEG 8k, 200 mM trisodium citrate·$2H_2O$, 100 mM Hepes-NaOH, pH 7.4, and 10 mM DTT) and transferred 2 h later to cryobuffer (22% (w/v) PEG 8k, 200 mM trisodium citrate·$2H_2O$, 100 mM Hepes-NaOH, pH 7.4, 10 mM DTT, and

TABLE I
Data collection, MAD data, and refinement statistics

Data collection statistics			
Space group/unit cell	C2	$a = 94.0\ b = 149.3\ c = 69.9\ \beta = 125.2$	
Dataset	Peak	Inflection	Remote
Wavelength (Å)	0.9818	0.9824	0.9716
Unique reflections	27,070	27,011	42,638
Redundancy	4.82	4.82	4.82
Resolution (Å)[a]	30.0–2.50 (2.59–2.50)	30.0–2.50 (2.59–2.50)	30.0–2.20 (2.28–2.20)
Completeness (%)[a]	98.7 (98.1)	98.7 (98.1)	98.4 (97.7)
Mean $I/\sigma(I)$[a]	16.3 (8.7)	16.2 (8.8)	14.5 (2.8)
R_{merge} (%)[a,b]	7.4 (36.0)	5.3 (30.5)	5.5 (37.7)

MAD data statistics						
	Peak		Inflection		Remote	
	Centric	Acentric	Centric	Acentric	Centric	Acentric
Phasing power[c]	2.48	1.91	1.82	1.391	2.125	1.718

Refinement statistics				
Resolution (Å)[a]	30–2.20			
Reflections	Working	37636	Free	1517
Total residues/waters	645/322			
R-factor[d]/R_{free}-factor[e]	21.8/24.7			
r.m.s.d.[f]	Bonds (Å)	0.007	Angles (°)	1.3

[a] Values in brackets are for outer resolution shell.
[b] $R_{merge} = (\Sigma_h\Sigma_j = 1, N|I_h - I_h\ (j)|/\Sigma_h N \times I_h)$ for the intensity of a reflection measured N times.
[c] Phasing power = $\Sigma|F_H|/\Sigma||F_{PH}(obs)| - |F_{PH}(calc)||$.
[d] $R = \Sigma_h\ ||F_{obs}| - k|F_{calc}||/\Sigma_h|F_{obs}|$, where F_{obs} and F_{calc} are the observed and calculated structure factor, respectively, and k is a scaling factor.
[e] R_{free} is identical to R on a subset of test reflections not used in refinement.
[f] r.m.s.d., root mean square deviation.

10% glycerol). After 18 h in this buffer, the crystal was frozen in a stream of liquid nitrogen gas at 100 K at the EMBL BW7a beamline at the DORIS storage ring, DESY (Hamburg, Germany). An x-ray fluorescence spectrum at the selenium K absorption edge was obtained by tuning the wavelength of the incident x-ray beam and used to determine the wavelengths necessary for subsequent data collection. A three-wavelength dataset was collected at the selenium peak (λ = 0.9818 Å), inflection point (λ = 0.9824 Å), and high energy remote (λ = 0.9716 Å), in that order. Data (360°) were collected for each wavelength, with 1° oscillation in each frame, but only 220° of data for each wavelength were used for structure determination. The data were processed with Denzo and Scalepack (18). The crystal belongs to space group C2 and has cell dimensions $a = 94.0$ Å, $b = 149.3$ Å, $c = 70.0$ Å, and $\beta = 125.2°$. The asymmetric unit contains one EF-Tu_{mt}·Ts_{mt} complex and has a solvent content of 52%.

Structure Determination—MAD phase calculation using all three wavelengths and subsequent structure refinement were carried out in CNS (19). Eleven of 12 possible SeMet sites in EF-Tu_{mt} were successfully located. The MAD phases were used as MLHL restraints in the initial cycles of refinement to 2.5-Å resolution. The density-modified experimental three-wavelength electron density map calculated at 2.5Å was easily interpretable. Upon refining to 2.2 Å, the target was switched to MLF, and refinement was carried out against the remote data without anomalous contribution. Models were visualized in O (20). Residues 44–55 and 84–111 of EF-Tu_{mt} had no density initially and could not be modeled after refinement. Residues 112, 117–119, 225–228, 251–256, 295–298, 310–314, and 452 of EF-Tu_{mt} initially had badly defined density but could be built after refinement. The region of EF-Tu_{mt} containing residues 182–187 had bad density even after refinement indicated by their high B-factors. SeMet 375 of EF-Tu_{mt} was observed to have a double conformation and was refined accordingly in the last step of refinement. EF-Ts_{mt} had poor density for residues 187–193 and no density for 330–338. During refinement, residues 187–193 and 330–331 were built. Residues 332–338 were the only ones that could not be built. A total of 322 water molecules were assigned to the asymmetric unit. The quality of the final model was inspected with PROCHECK (21), and the secondary structure was assigned with DSSP (22). The final model, having been refined from 30.0 to 2.2 Å, has a $R_{work} = 21.8\%$ and a $R_{free} = 24.7\%$. The root mean square deviation for bond lengths is 0.007 Å and 1.3° for bond angles. There are no outliers in the Ramachandran plot, and there are only 4 residues in the generously allowed region from a total of 645 residues. See Table I for data collection and refinement statistics. Fig. 1, *A* and *B*, and Figs. 4–6 were made with PyMOL (23).

RESULTS

Overall Structure—The crystallographic asymmetric unit contains one heterodimeric complex of EF-Tu_{mt}·Ts_{mt}, and 322 water molecules could be modeled. The overall structure of the complex (Fig. 1*A*) is similar to that of the *E. coli* EF-Tu·Ts complex (14). As in the *E. coli* complex, the amino-terminal domain and subdomain N of EF-Ts_{mt} contact domain I of EF-Tu_{mt}, whereas subdomain C interacts with domain III. The buried surface area, when considering these contacts, constitutes 3140 Å^2 in the mitochondrial complex compared with 2623 Å^2 in the *E. coli* complex. When also considering the contacts made between domain I and the carboxyl-terminal module in the *E. coli* complex, the buried surface area in this complex is 3624 Å^2. This kind of interaction is not observed in the mitochondrial complex because EF-Ts_{mt} is shorter than *E. coli* EF-Ts and the last 7 residues could not be modeled in the mitochondrial protein.

EF-Ts_{mt}—The structure of EF-Ts is known for both the *E. coli* and *T. thermophilus* factors (14, 15). The structure of *E. coli* EF-Ts has been divided into five domains, the amino-terminal domain, subdomains N and C of the core region, the coiled-coil region (which is part of the dimerization domain), and the carboxyl-terminal module. There is a duplication of the secondary structure motif in subdomain N and C that gives rise to a local internal pseudo-symmetry (Fig. 1, *B* and *C*). The corresponding structure of the dimeric *T. thermophilus* EF-Ts is created by the three-stranded anti-parallel β-sheet on each subunit interacting to form a truly symmetric β-sandwich corresponding to the β-sandwich structure observed between subdomain N and C of the core of *E. coli* EF-Ts (24).

The basic structure of EF-Ts_{mt} has interesting similarities and also rather striking differences compared with that of the *E. coli* factor (Fig. 1, *B* and *C*). In contrast to *T. thermophilus* EF-Ts, both *E. coli* and mitochondrial EF-Ts function as monomers in solution, and comparisons will therefore be made between the mitochondrial and *E. coli* factors. Overall, the amino-terminal domain is similar between the two factors. The two

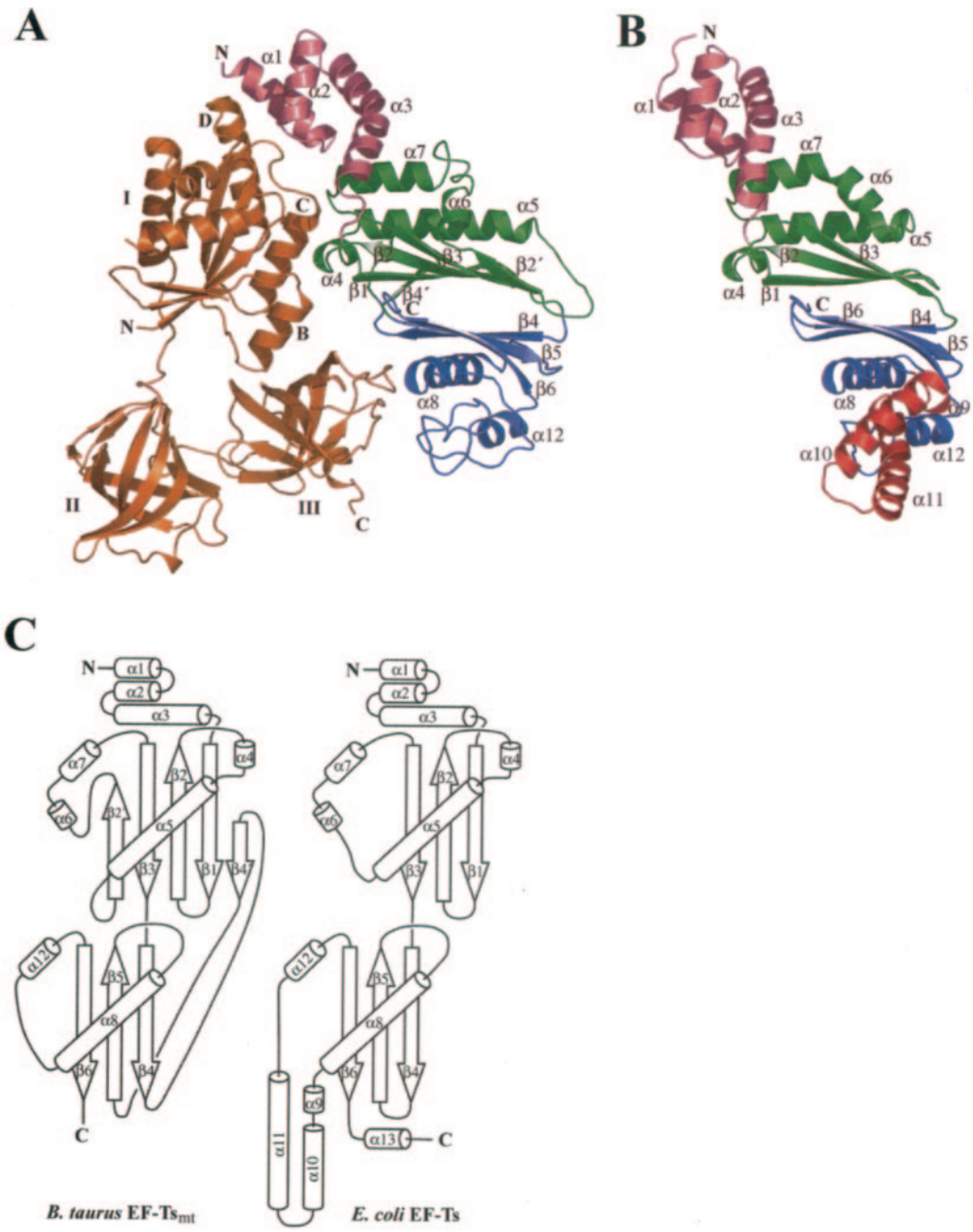

FIG. 1. *A*, cartoon representation of the bovine EF-Tu$_{mt}$·Ts$_{mt}$ complex. EF-Tu$_{mt}$ is colored *orange*, and EF-Ts$_{mt}$ is colored *violet* (amino-terminal domain), *green* (subdomain N), and *blue* (subdomain C). The amino terminus and carboxyl terminus of both proteins are labeled along with domain I, II, and III and helices B, C, and D of EF-Tu$_{mt}$ and the secondary structure elements of EF-Ts$_{mt}$. Not shown in cartoon are four 3_{10}-helices of EF-Ts$_{mt}$ (see the Fig. 2 legend). *B*, cartoon of *E. coli* EF-Ts (helix α13 and connecting loop have been omitted for clarity) (14). The overall structure of the *E. coli* EF-Ts molecule is very similar to that of bovine EF-Ts$_{mt}$. It has been colored as described for the domains of EF-Ts$_{mt}$, and additionally, the *E. coli* EF-Ts coiled-coil motif consisting of helices α9, α10, and α11 is shown in *red*. *C*, secondary structure projection of the bovine EF-Ts$_{mt}$ and *E. coli* EF-Ts structures. Secondary structure elements common with *E. coli* EF-Ts are named as in *E. coli* EF-Ts. In bovine EF-Ts$_{mt}$, the amino-terminal domain consists of α1, α2, and α3; subdomain N consists of β1, β2, α4, α5, β2′, α6, α7, β3, and β4′; and subdomain C consists of β4, β5, α8, α12, and β6.

structures then begin to show some deviations. The cores of *E. coli* EF-Ts and EF-Ts$_{mt}$ are both formed by a β-sandwich. However, the number of β-strands and their arrangement differ between them. Most dramatically, the coiled-coil domain found in *E. coli* EF-Ts (helices α9, α10, and α11 in Fig. 1*B*) is almost completely eroded in the mitochondrial factor (Fig. 1*A*, loop region between α8 and α12).

The amino-terminal domain of bovine EF-Ts$_{mt}$ is structurally similar to the amino terminus of the EF-Ts from both *E. coli* and *T. thermophilus* (14, 15). It consists of the helical segments α1-α3 (Fig. 1, *A* and *C*). The insertion of 4 extra residues in the bovine protein located in helix α3 adds one helical turn to this helix and moves the amino-terminal domain slightly closer to helix D of EF-Tu$_{mt}$ compared with EF-Ts in the two other complexes. Helix α3 has a considerable kink in its middle at sAla^{99} (in the following sections, residues will be referred to by the prefixes u and s if they belong to EF-Tu or EF-Ts, respectively). The kink in the mitochondrial factor is more pronounced than that seen in *E. coli* at sGly^{44}, whereas α3 is only slightly bent in *T. thermophilus* EF-Ts.

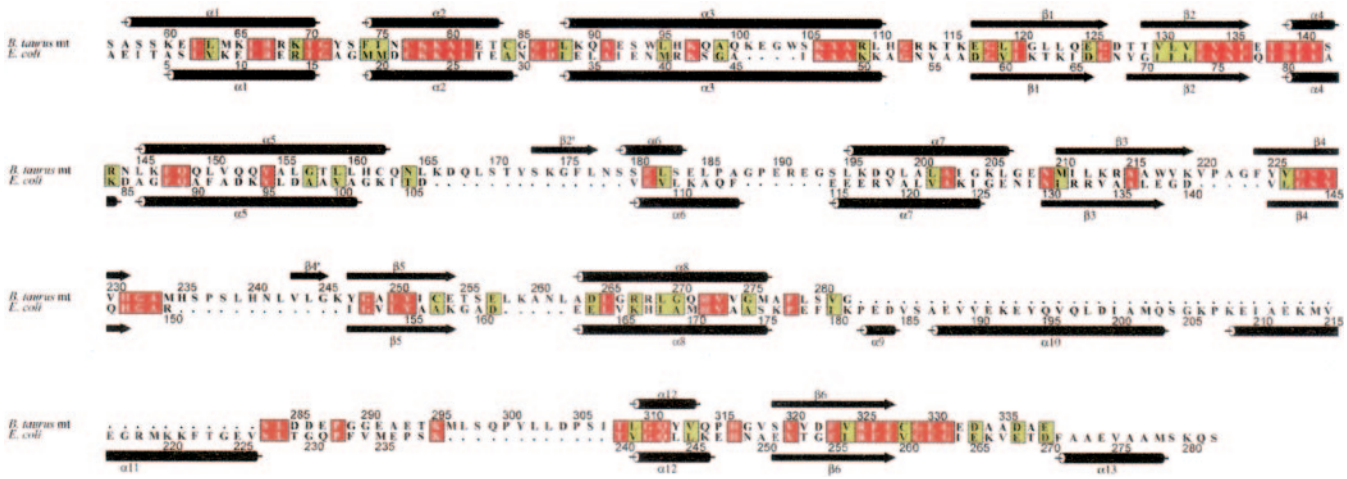

FIG. 2. **Structural sequence alignment of EF-Ts from *B. taurus* mitochondria and *E. coli* showing the secondary structural elements for the mitochondrial and *E. coli* factors.** The definitions of secondary structure elements of bovine EF-Ts_{mt} are as follows: α1, 57–70; α2, 74–83; α3, 88–110; β1, 117–125; β2, 128–136; α4, 139–142; α5, 145–162; $\beta2'$, 173–177; α6, 179–183; α7, 195–206; β3, 210–219; β4, 224–231; $\beta4'$, 243–245; β5, 247–254; α8, 263–276; α12, 309–313; and β6, 319–327. There are also four 3_{10}-helices in EF-Ts_{mt} (residues 259–261, 290–292, 296–298, and 314–316). The numbering for EF-Ts_{mt} reflects the residues in the precursor. The numbering for *E. coli* EF-Ts begins with the Ala, reflecting the removal of the amino-terminal methionine in the native protein. The structure of the mitochondrial EF-Ts_{mt} does not include the last 7 residues shown in the sequence.

Subdomain N of EF-Ts_{mt} consists of four helical segments (α4-α7) and a five-stranded β-sheet (β1, β2, $\beta2'$, β3, and $\beta4'$) (Fig. 1, *A* and *C*). In *E. coli* EF-Ts, subdomain N of the core consists of four helical segments (α4-α7) and a three-stranded β-sheet (β1-β3) (Fig. 1*B*). Helix α3 from the amino-terminal domain leads into β-strand β1 in subdomain N of the core. This strand makes a turn and runs anti-parallel to strand β2. Strand β2 is followed by a short helix, α4, which contains the important aspartic acid and phenylalanine residues that play a role in the nucleotide exchange reaction. This section then leads into helix α5. In *E. coli* EF-Ts, α5 is followed by another helical segment (α6). However, in EF-Ts_{mt}, there is a large insertion of residues between helices α5 and α6, creating an extra β-strand ($\beta2'$) consisting of five residues that runs anti-parallel to β-strand β3 (Fig. 1*C*). The polypeptide chain then turns ~90° perpendicular to the β-sheet and forms a short helix (α6) consisting of 5 residues. This helix is followed by a loop remarkably similar in size and shape to the one found in *T. thermophilus* EF-Ts between helices α7 and α8 (15) and distinct from the corresponding region in *E. coli* EF-Ts, where α6 leads directly into α7 (Figs. 1 and 2). The loop in EF-Tu_{mt} is followed by a helix that corresponds to α7 in *E. coli* EF-Ts. This helix leads into the last β-strand, β3, of the β-sheet in subdomain N.

Subdomain C of the core of EF-Ts_{mt} begins where strand β3 leads into strand β4 (Fig. 1). An insertion of 3 residues between β3 and β4 compared with *E. coli* EF-Ts extends these strands in bovine EF-Ts_{mt} and stabilizes the amino terminus of strand $\beta2'$ in the mitochondrial factor. In *E. coli* EF-Ts, strand β4 leads directly into strand β5. In EF-Ts_{mt}, there is another insertion between β4 and β5 that folds back across the pseudo 2-fold symmetry axis of EF-Ts to subdomain N of the core domain. It forms a loop and a small β-strand, $\beta4'$, consisting of 3 residues. It is fixed in place by hydrogen bonds to β1, and the chain then returns back to form strand β5 in subdomain C of the core domain. This organization means that the β-sheet in subdomain N of the core consists of five β-strands, instead of three β-strands as in the other two EF-Tu·Ts complexes. Residues 255–262 form a loop between β5 and α8 that contains a 3_{10}-helix (residues 259–261) (data not shown). This loop is similar to but 2 residues shorter than the one seen in *T. thermophilus* EF-Ts between β2 and α5 of the second EF-Ts moiety of the $(EF\text{-}Tu\cdot Ts)_2$ complex (15). In *T. thermophilus*, this region contains the conserved TDFV sequence motif that interacts with EF-Tu.

The region between helices α8 and α12 corresponding to the coiled-coil segment in *E. coli* EF-Ts is reduced to a large loop in bovine EF-Ts_{mt} that packs against subdomain C of the core domain (Fig. 1*A*). Due to the less well defined density at the carboxyl terminus of mitochondrial EF-Ts_{mt} following $sGly^{331}$, the last 7 residues of EF-Ts_{mt} could not be modeled. In the *E. coli* EF-Ts structure, this region is followed by a loop and an additional helix, α13, which interacts with domain I of EF-Tu. The carboxyl terminus of *T. thermophilus* EF-Ts is found at the position to which EF-Ts_{mt} could be modeled.

The EF-Tu_{mt}·Ts_{mt} Interface—There are basically three major areas of contact between EF-Tu_{mt} and EF-Ts_{mt}, two regions involving contacts with domain I and one major region contacting domain III of EF-Tu_{mt}. The amino-terminal domain of EF-Ts_{mt} interacts with residues in helix D and the loop leading into helix C of domain I of EF-Tu_{mt}. Subdomain N of the core contacts EF-Tu_{mt} through residues in helix C and the region between helices B and C. Finally, subdomain C of the core makes contacts with domain III of EF-Tu_{mt}.

Contacts between the amino-terminal domain of EF-Ts_{mt} and domain I of EF-Tu_{mt} result in a significant displacement of helix D, which moves away from domain III. Helix α1 from the amino terminus of bovine EF-Ts_{mt} interacts primarily with helix D of EF-Tu_{mt} (Fig. 3*A*). The methylene groups from the side chain of $sLys^{60}$, $sLeu^{63}$, $sMet^{64}$, and $sPhe^{74}$ form a hydrophobic pocket for $uLeu^{194}$. Numerous electrostatic contacts are also present (Fig. 3*A*). The side chain of $uGlu^{190}$ is within hydrogen bonding distance with the amino-terminal amine of $sSer^{56}$ (the amino-terminal residue of the mature protein) and its carbonyl oxygen (Fig. 3*A*). Residue $sLys^{60}$ forms a salt bridge to $uGlu^{193}$ $O\epsilon_1$. The side chain of residue $sArg^{67}$ forms a hydrogen bond to the backbone carbonyl of $uPro^{157}$ and $sTyr^{72}$ and is further fixed in place by salt bridges with $uGlu^{198}$ through $O\epsilon_1$ to $N_{\eta 2}$ and $O\epsilon_2$ to N_ϵ. The side chain of $sArg^{68}$ forms salt bridges with $uGlu^{201}$ through $N_{\eta 1}$ to $O\epsilon_1$ and $N_{\eta 2}$ to $O_{\epsilon 2}$. Residues $sLeu^{63}$, $sPhe^{74}$, and the aliphatic part of $sLys^{78}$ form a hydrophobic patch that accommodates the side chain of $uMet^{191}$. An electrostatic interaction takes place between $sLys^{78}$ and $uAsp^{188}$ $O_{\gamma 2}$ (3.6 Å). The backbone amide of $sPhe^{74}$

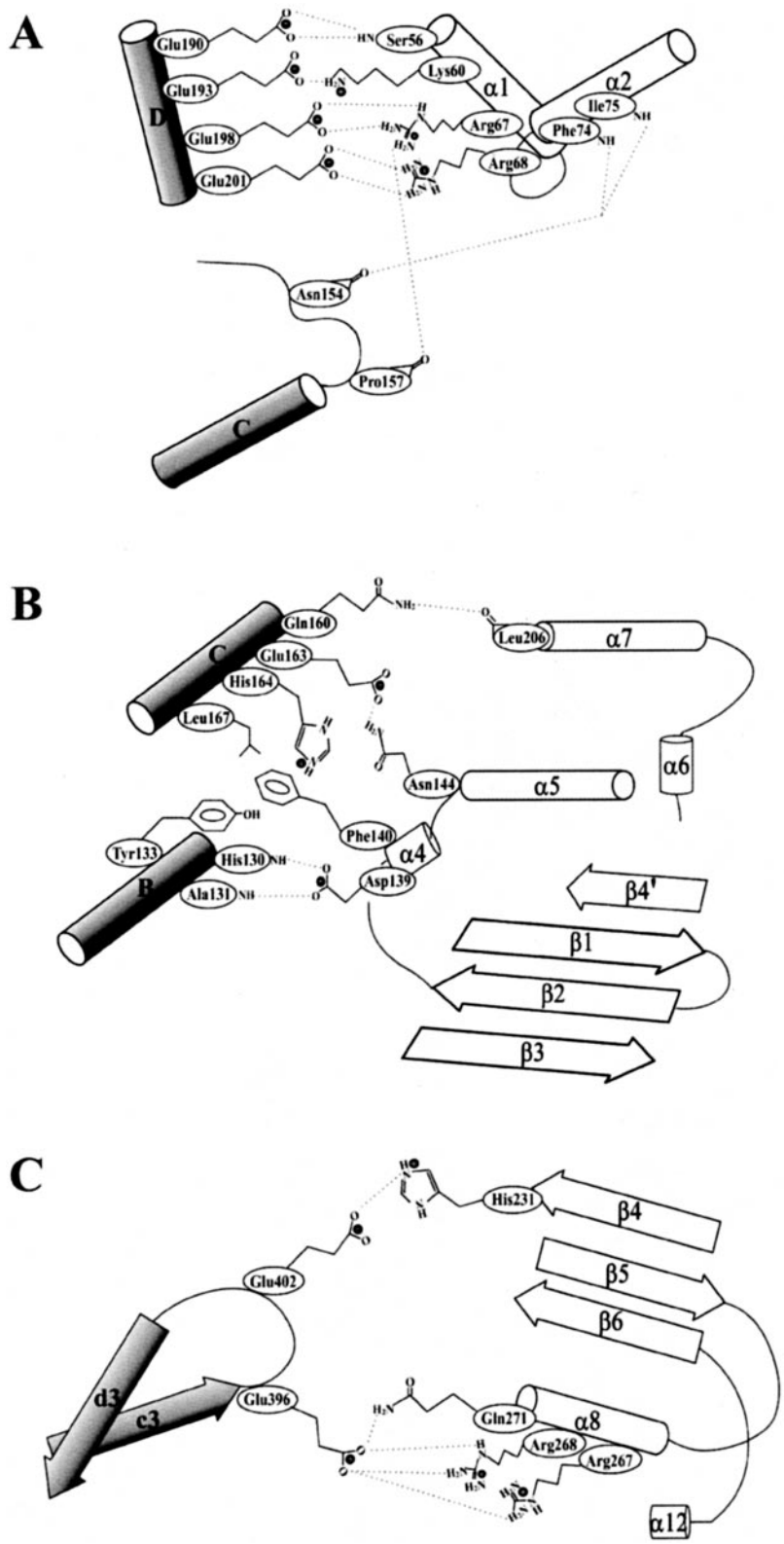

FIG. 3. **Schematic diagram showing some of the interactions in the bovine EF-Tu_{mt}·Ts_{mt} interface.** *A*, electrostatic and hydrogen bond interactions between residues in the amino-terminal domain of EF-Ts_{mt} and domain I of EF-Tu_{mt}. Hydrophobic interactions are also present in this region (see "Results"). *B*, subdomain N of the core interactions near helices B and C in EF-Tu_{mt}. Hydrogen bond and electrostatic interactions are shown. *C*, interactions between subdomain C of the core of EF-Ts_{mt} and domain III of EF-Tu_{mt}. The electrostatic and hydrogen bond interactions are illustrated here. Note that there are considerable hydrophobic contacts in this region (see "Results"). See also Fig. 6.

and sIle^{75} from the amino terminus of helix α2 of EF-Ts_{mt} makes hydrogen bonds with the backbone carbonyl of residue uAsn^{154} from the loop leading to helix C of EF-Tu_{mt}.

Subdomain N of the core of EF-Ts_{mt} plays a critical role in the rearrangements in EF-Tu_{mt} that lead to the release of the bound nucleotide. Residue sPhe^{140} from the conserved TDFV sequence motif found in all EF-Ts sequences is inserted directly between helices B and C of EF-Tu_{mt} as observed in the *E. coli* and *T. thermophilus* complexes (Figs. 3*B* and 6). The conserved Asp residue (sAsp^{139} in EF-Ts_{mt}) makes tight hydrogen bond contacts with the backbone amides of uHis^{130} (2.8 Å) and uAla^{131} (3.1 Å) of helix B (Fig. 3*B*). Residue sAsn^{144} in the loop between α4 and α5 of EF-Ts_{mt} makes a hydrogen bond contact with uGlu^{163} in helix C of EF-Tu_{mt}. In addition, the backbone carbonyl of sLeu^{206} at the very end of α7 in EF-Ts_{mt} makes hydrogen bonds with the side chain of uGln^{160} at the end of helix C in EF-Tu_{mt} (Fig. 3*B*). A slight difference in the coordination of the P-loop in domain I of EF-Tu by EF-Ts can be

observed among the mitochondrial, *E. coli*, and *T. thermophilus* complexes. The mitochondrial residues sArg^{109} and sArg^{113} from α3 coordinate the carboxyl side chain of mitochondrial uAsp^{67}. In *E. coli*, sLys^{51} coordinates uAsp^{21}, whereas *T. thermophilus* EF-Ts has both sLys^{50} and sArg^{53} contacting uAsp^{21}.

Subdomain C of the core of EF-Ts$_{mt}$ contacts domain III of EF-Tu$_{mt}$. The relative position of domain III of EF-Tu$_{mt}$ in relation to subdomain C of the EF-Ts$_{mt}$ core is different from that in the *E. coli* complex. When helices B and C from EF-Tu$_{mt}$ and the regions from the core of EF-Ts$_{mt}$ that interact with EF-Tu$_{mt}$ are superimposed, there is a rotation of ~18° of domain III around helix B in a clockwise manner when looking from the amino terminus toward the carboxyl terminus of this helix. The difference is minimal at the interface to EF-Ts$_{mt}$ and progresses further away from the domain III/EF-Ts$_{mt}$ interface. In comparison, the *E. coli* and *T. thermophilus* complexes superimpose almost perfectly for domains II and III. A hydrophobic patch on EF-Tu$_{mt}$ consisting of the methylene groups of uLys^{368}, uPro^{369}, uVal^{371}, uLeu^{397}, and uMet^{399} faces residues sGly^{275}, sMet^{276}, sLeu^{302}, and sLeu^{303} on EF-Ts$_{mt}$. The carboxylic oxygens of uGlu^{396} are held in place by interactions from sGln^{271} Nϵ_2 and sArg^{267} N$_{\eta 2}$ and more weakly by sArg^{268} Nϵ and sArg^{268} N$_{\eta 2}$ (Fig. 3*C*). There is also contact between sHis^{231} at the end of β4 and uGlu^{402} in the loop between strands c3 and d3 in EF-Tu$_{mt}$. The side chain hydroxyl group of sTyr^{229} stabilizes sHis^{231} through a hydrogen bond to Nδ_1.

EF-Tu$_{mt}$—The conformation of bovine EF-Tu$_{mt}$ in complex with EF-Ts$_{mt}$ is distinct from the EF-Tu$_{mt}$·GDP complex (10). When superimposing domain III of bovine EF-Tu$_{mt}$ in the GDP and EF-Ts$_{mt}$ complexed forms, helix B in domain I in the two structures is almost superimposed (Fig. 4*A*). However, the remainder of domain I is rotated ~25° as a rigid body relative to this helix away from domain III toward domain II. The solvent-accessible surface of EF-Tu$_{mt}$ from the EF-Ts$_{mt}$ complex decreases by 140 Å^2 compared with the GDP-bound form as a result of the movement of the carboxyl-terminal part of helix C away from domain III. Besides the changes in the P-loop and near the guanine nucleotide binding site, which will be described later, there are no changes in this domain. This is similar to the changes observed in domain I of *E. coli* EF-Tu between the GDP and EF-Ts complexed forms (12, 14). Surprisingly, domain II of EF-Tu$_{mt}$ in the EF-Tu$_{mt}$·Ts$_{mt}$ complex is also rotated ~18° as a rigid body toward domain I relative to domain III when compared with the EF-Tu$_{mt}$·GDP complex (Fig. 4*A*). This rotation is exemplified by the movement of the loop between β-strands b2 and c2 in domain II by ~7.8 Å. The shape of the "hole" between the three domains of EF-Tu$_{mt}$ is slightly altered, mainly as a result of the relative movements of domain I and the linker between domains I and II. The rotation of domain II is probably a result of the movement of domain I, which mediates its effect through the linker between these two domains, because there are no major changes in domain III.

As a result of the domain rearrangements, some of the interface interactions between domain II and III have changed upon EF-Tu$_{mt}$·Ts$_{mt}$ complex formation from the EF-Tu$_{mt}$·GDP complex (Fig. 4*B*). In the EF-Tu$_{mt}$·GDP structure, residues uHis^{295} and uSer^{296}, from the loop between β-strands e2 and f2, of domain II interact with residues uMet^{385}, uGln^{412}, uPro^{413}, and uMet^{414} from domain III (10). Residue uHis^{295} is held in place by uMet^{385} and uMet^{414} from domain III and uArg^{335} from domain II. In the EF-Tu$_{mt}$·Ts$_{mt}$ complex, the peptide bond between uGly^{294} and uHis^{295} has flipped ~170°, causing the following residues in the loop to assume a different conformation than that observed in the EF-Tu$_{mt}$·GDP complex. The relative movement of the C$_\alpha$ atoms of uHis^{295} and uSer^{296} is 6.1 and 5.8 Å, respectively, when domain III is superimposed in the two structures. In the equivalent *E. coli* structures, there is essentially no change between the relative positions of domain II and III upon complex formation with EF-Ts (12, 14). The interface between domains II and III is also basically the same in the *E. coli* EF-Tu·GDPNP·Phe-tRNA·kirromycin complex,[2] indicating that in the bacterial EF-Tu, these domains act together as a rigid body. The loop between β-strands e2 and f2 in domain II of EF-Tu$_{mt}$ is similar but not identical in shape or position to the corresponding region in domain II of the *T. thermophilus* EF-Tu·Ts complex (15).

Rearrangements Leading to Guanine Nucleotide Exchange—The dramatic conformational changes observed in domain I of EF-Tu$_{mt}$ are critical for the nucleotide exchange process. The changes lead to the disruption of the binding site for the guanine nucleotide. The changes observed encompass portions of EF-Tu$_{mt}$ that interact with the guanine base and regions binding the β-phosphate and Mg^{2+} ion. The GTP-binding site is defined by three consensus sequence elements (for review, see Ref. 26). The first sequence motif, G*XXXX*GK(S/T), also called the P-loop, coordinates the α- and β-phosphate groups of the bound nucleotide. The second motif, D*XX*G, which is part of the switch II region, is involved in the coordination of the γ-phosphate. The third motif, NK*X*D, determines the specificity for the guanine base. Furthermore, a conserved threonine residue from the switch I region coordinates the Mg^{2+} ion.

The mechanism of guanine nucleotide exchange in EF-Tu is suggested to occur through a three-part mechanism. The interaction between EF-Tu and EF-Ts results in the disruption of the Mg^{2+} ion binding site that is induced by the intrusion of the side chains of Asp^{80} and Phe^{81} (*E. coli* numbering) from EF-Ts between helices B and C in domain I of EF-Tu. A peptide flip in the P-loop of EF-Tu destabilizes the binding of one β-phosphate oxygen of GDP, and the movement of EF-Tu helix D affects the binding of the sugar and base of the bound nucleotide.

The region in EF-Tu$_{mt}$ (K^{182}ADAVQ^{187}) containing part of the conserved NK*X*D motif involved in nucleotide binding was very difficult to model and had less well defined density even after the final refinement. The orientation of this loop is different from that of the EF-Tu$_{mt}$·GDP complex (Fig. 5). In *E. coli*, sLys^{23} in the amino-terminal domain of EF-Ts makes an electrostatic contact with uAsp^{141} from the loop following the NK*X*D motif. In EF-Tu$_{mt}$, the aspartic acid residue found in *E. coli* EF-Tu (uAsp^{141}) is replaced by uGln^{187} that points in a different direction than in the *E. coli* protein. The side chain of uGln^{187} forms two hydrogen bonds with the side chain of uAsn^{154} in the mitochondrial EF-Tu$_{mt}$·Ts$_{mt}$ complex. The mitochondrial residue equivalent to *E. coli* sLys^{23} (sLys^{78}) is conserved in EF-Ts$_{mt}$ but makes a salt bridge with uAsp^{188} (3.6 Å). A similar orientation of the equivalent of EF-Tu$_{mt}$ uLys^{182} is seen in two other G-proteins complexed with their nucleotide exchange factor, namely, that of Ras·Sos1 and Ran·RCC1 (27, 28). The conformation observed in the EF-Tu$_{mt}$·Ts$_{mt}$ complex could represent a state in the exchange mechanism distinct from that observed in the *E. coli* and *T. thermophilus* complexes.

As mentioned, two of the dominant residues in the interaction between EF-Tu and EF-Ts are from the conserved TDFV motif in subdomain N of the core of bovine EF-Ts$_{mt}$, namely, sAsp^{139} and sPhe^{140} (Figs. 3*B* and 6). The phenyl ring of sPhe^{140} sits in a hydrophobic region with uTyr^{133} and uLeu^{167} and between the side chains of uHis^{130} and uHis^{164}. This position inserts sPhe^{140} between helices B and C and clearly disrupts the binding site for the Mg^{2+}·GDP. Residues 84–111 containing the switch I region of EF-Tu$_{mt}$ could not be modeled.

[2] R. C. Nielsen, O. Kristensen, M. Kjeldgaard, S. Thirup, J. Nyborg, and P. Nissen, manuscript in preparation.

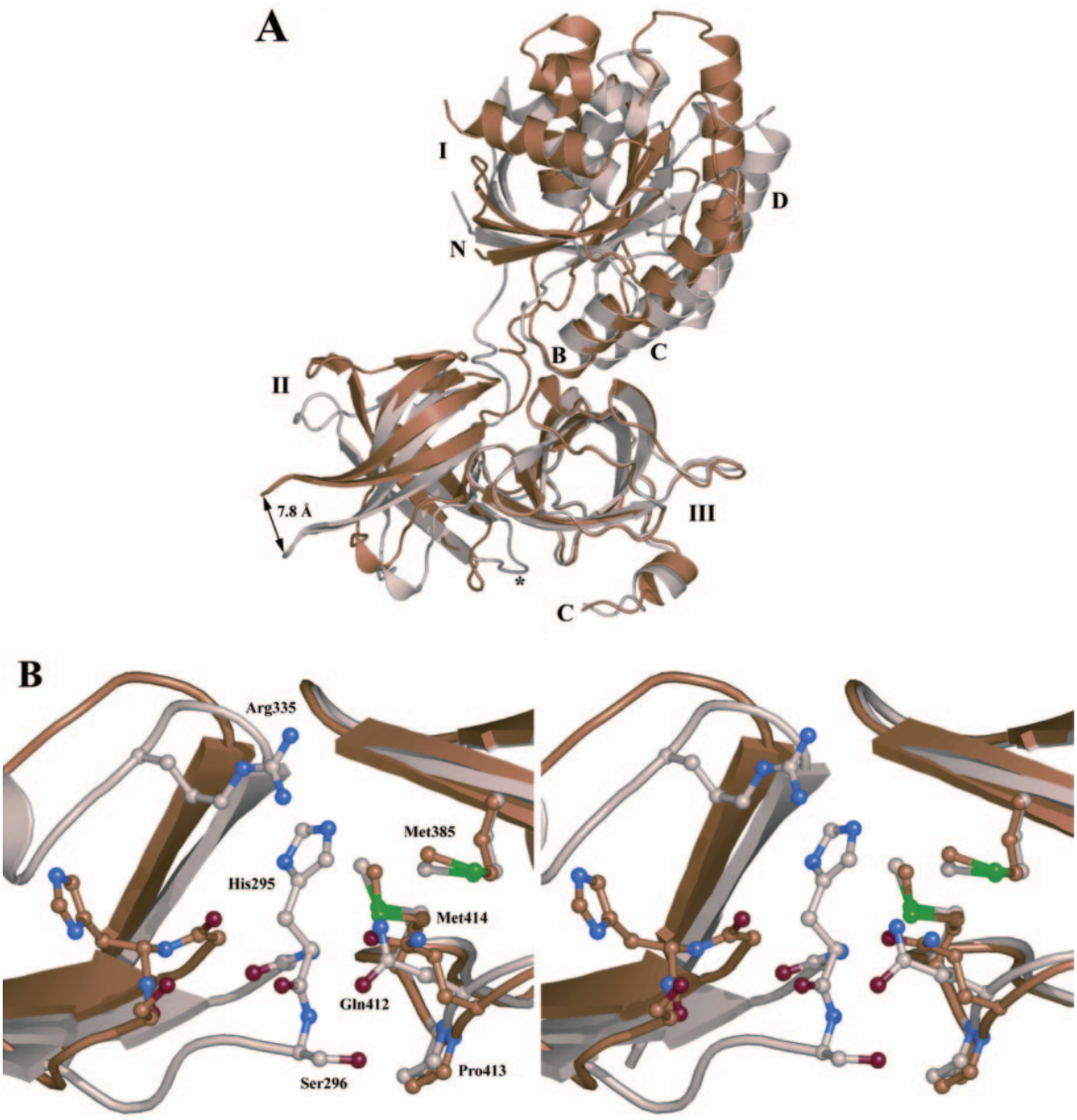

FIG. 4. *A*, superposition of EF-Tu_{mt} domain III from EF-Tu_{mt}·GDP and the EF-Tu_{mt}·Ts_{mt} complex viewed from the EF-Tu_{mt}·Ts_{mt} interface. EF-Ts_{mt} has been removed for clarity. EF-Ts_{mt} complexed EF-Tu_{mt} is colored *orange*, and EF-Tu_{mt} in the GDP conformation is shown in *wheat*. Residues 84–111 of the EF-Tu_{mt}·GDP complex have been omitted for clarity. Helices B, C, and D of domain I of EF-Tu_{mt} are labeled. Helix B from domain I superimposes well in the two conformations. The rest of domain I is rotated/twisted away from domain III by ~25°. Note the movement of domain II in the background. *B*, stereo-view of the interface between domain II and III of EF-Tu_{mt} around the loop of domain II marked by an *asterisk* in *A* (not all secondary structure is shown). Domain II is seen at the *left*, and domain III is seen at the *right*, with the same coloring as described in *A*. Selected residues have been labeled. The C_α atom of $uHis^{295}$ moves by ~6.1 Å. See "Results" for further explanation.

This region is involved in large conformational changes between the GDP- and GTP-bound state of EF-Tu (29, 30). A peptide flip between residues $uVal^{66}$ and $uAsp^{67}$ causes the P-loop to change conformation as seen in other complexes of G-proteins and their exchange factors (14, 15, 31).

Mutations versus Structure—A number of mutations have been made in residues of EF-Ts_{mt} that were predicted to interact with EF-Tu_{mt}. These predictions were based on the alignment of the sequences of the bacterial and mitochondrial factors and on the structure of the *E. coli* EF-Tu·Ts complex (14, 32–34). The variants made have been divided into three groups, based on their location in the structure of EF-Ts (Table II and Fig. 6). The first group is located in the amino-terminal domain. In the *E. coli* EF-Tu·Ts complex, $sArg^{12}$ makes an electrostatic contact with $uGlu^{152}$ and a hydrogen bond with the backbone carbonyl of $uPro^{111}$ (3.4 Å). It plays an essential role in the interaction of these two factors (32). The corresponding position in EF-Ts_{mt} is $sArg^{67}$. This residue makes electrostatic interactions with $uGlu^{198}$ and a hydrogen bond contact with the backbone carbonyl of $uPro^{157}$ (2.9 Å). The adjacent residue $sArg^{68}$ makes salt bridge contacts with $uGlu^{201}$ in helix D of EF-Tu_{mt} (Fig. 3*A*). However, a triple mutant in this region of mitochondrial EF-Ts_{mt} (R67A, R68A, and K69A) that eliminates these interactions is as active as wild-type EF-Ts_{mt}. Hence, unlike the *E. coli* complex, these interactions between EF-Tu_{mt} and EF-Ts_{mt} do not contribute significantly to the guanine nucleotide exchange in the mitochondrial system.

Contacts between helix $\alpha 2$ in the amino-terminal domain of EF-Ts_{mt} and helix D in domain I of EF-Tu_{mt} also were predicted to involve residues $sPhe^{74}$ and $sIle^{75}$. In the crystal

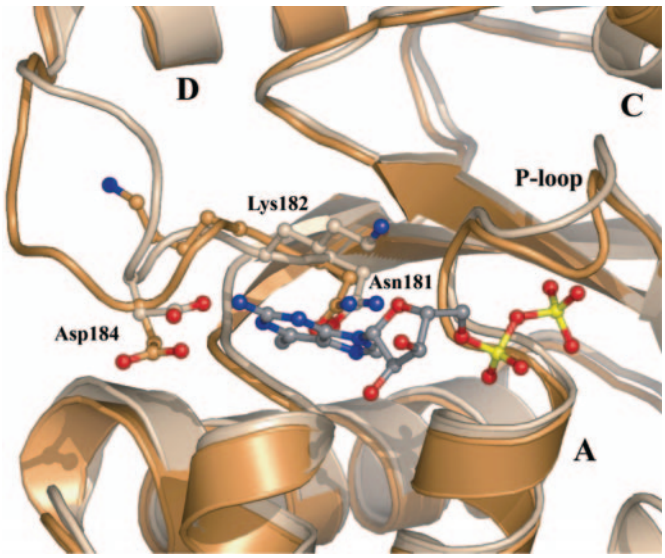

FIG. 5. **Conformational changes at the guanine base binding site in domain I of EF-Tu$_{mt}$.** EF-Tu$_{mt}$·GDP and the EF-Tu$_{mt}$·Ts$_{mt}$ complex are colored *wheat* and *orange*, respectively. The GDP moiety is shown in *gray stick representation*, with nitrogens colored *blue*, oxygens colored *red*, and phosphorus colored *yellow*. Residues uAsn^{181}, uLys^{182}, and uAsp^{184} from the NKXD motif (also shown in *stick representation*), along with helices A, C, and D and the P-loop, have been labeled. The loop following the NKXD motif in EF-Tu$_{mt}$ is in a distinct conformation after complex formation with EF-Ts$_{mt}$. The P-loop, as in other G-protein·nucleotide exchange factor complexes, is seen to have a different conformation due to a peptide flip in this loop.

structure of the bovine EF-Tu$_{mt}$·Ts$_{mt}$ complex, sPhe^{74} makes hydrophobic contacts with the side chains projecting from helix D of EF-Tu$_{mt}$, although it is not tightly nestled in this pocket. The backbone amide group of sPhe^{74} forms a weak hydrogen bond to the backbone carbonyl oxygen of uAsn^{154} on EF-Tu$_{mt}$ (3.3 Å). The backbone amide group of sIle^{75} also hydrogen bonds to the backbone carbonyl oxygen of uAsn^{154} (3.2 Å), and its side chain may make a hydrophobic contact with the C$_\beta$-methylene of this residue. Three different mutants in these residues have been made (Table II) (34). Conversion of both sPhe^{74} and sIle^{75} to alanine results in a 2-fold reduction in the activity of EF-Ts$_{mt}$, suggesting that the hydrophobic interactions play some role in stabilizing the interaction of EF-Ts$_{mt}$ with EF-Tu$_{mt}$. Replacement of both residues with methionine converts this sequence into one identical to that observed in *E. coli* EF-Ts. This variant has an activity indistinguishable from that of the wild-type factor. Clearly, a methionine at both positions is sufficient to maintain strong contacts between these two factors, allowing GDP exchange to occur readily. It is essential to maintain hydrophobic residues in this region because replacement of sPhe^{74} and sIle^{75} with glutamic acid residues completely inactivates EF-Ts$_{mt}$.

Mutational analysis shows that mutation of sLys^{78} and sLys^{79} to alanine in EF-Ts$_{mt}$ has no effect on the activity of EF-Ts$_{mt}$ (Table II). Based on the structural information, the mutation of sLys^{78} could be expected to destabilize the interaction of EF-Ts$_{mt}$ with the amino-terminal of helix D following the NKXD motif in EF-Tu$_{mt}$. Apparently, however, this contact is not important. The adjacent sLys^{79} points away from EF-Tu$_{mt}$, and its mutation is not expected to have an effect on the activity of EF-Ts$_{mt}$.

Mutation of either sAsp^{139} or sPhe^{140} from the conserved TDFV motif of EF-Ts$_{mt}$ to alanine reduces the activity of EF-Ts$_{mt}$ about 5-fold (Table II). This observation indicates that disruption of this region of EF-Tu$_{mt}$ plays a role (although not an essential one) in the ability of EF-Ts$_{mt}$ to promote guanine nucleotide exchange on EF-Tu$_{mt}$. Replacement of both sAsp^{139} and sPhe^{140} with alanine completely inactivates EF-Ts$_{mt}$, demonstrating that EF-Ts$_{mt}$ must be able to disrupt the region between helices B and C in EF-Tu$_{mt}$ to promote nucleotide exchange. The mutation of both these residues to alanine does not completely inactivate *E. coli* EF-Ts, indicating that they are not essential for the function of the bacterial factor (33).

EF-Ts$_{mt}$ interacts with domain III of EF-Tu$_{mt}$ over a significant surface (924 Å^2). One residue predicted to be important in this region of contact is sHis^{231} located in subdomain C of the core of EF-Ts$_{mt}$ (Figs. 3*C* and 6). The side chain of this residue interacts with the loop between β-strands c3 and d3 of domain III. The Nϵ_2 of the imidazole ring of sHis^{231} hydrogen bonds to an oxygen of uGlu^{402}, and Nδ_1 is hydrogen bonded to sTyr^{229}, whereas hydrophobic contacts are made with the side chains of uLeu^{397} and uMet^{399}. Mutation of sHis^{231} to alanine results in the loss of the side chain hydrogen bond and leads to a 6-fold reduction in the ability of EF-Ts$_{mt}$ to stimulate the activity of EF-Tu$_{mt}$ (Table II). Subdomain C also makes significant hydrophobic contacts with domain III of EF-Tu$_{mt}$. Two of these contacts involve sLeu^{302} and sLeu^{303}. Conversion of these residues to valine and methionine, respectively (the residues found in *E. coli* EF-Ts), had no effect on the activity of EF-Ts$_{mt}$. This observation is reasonable because these changes maintain the hydrophobic interactions between the two factors. However, conversion of the two residues to glutamic acids completely inactivated EF-Ts$_{mt}$, indicating that the hydrophobic contacts between EF-Ts$_{mt}$ and domain III of EF-Tu$_{mt}$ are essential for their interaction, as seen in the *E. coli* complex (34).

There are hydrogen bond contacts between sArg^{267} and sArg^{268} of EF-Ts$_{mt}$ and uGlu^{396} of EF-Tu$_{mt}$. However, mutation of both sArg^{267} and sArg^{268} to alanines did not affect the ability of EF-Ts$_{mt}$ to promote guanine nucleotide exchange with EF-Tu$_{mt}$, indicating that these contacts do not play a significant role in the interaction between these two factors.

DISCUSSION

One of the striking differences between EF-Ts$_{mt}$ and *E. coli* EF-Ts is the loss of the majority of the coiled-coil domain in the mitochondrial factor. The deletion of the coiled-coil motif in *E. coli* EF-Ts affects its ability to compete with guanine nucleotides for binding to EF-Tu (35). The concentration of either GDP or GTP needed to dissociate the mutant EF-Tu·Ts complex was 2 orders of magnitude lower than that for the wild-type complex. Furthermore, an *E. coli* strain harboring the EF-Ts mutant is resistant to phage Qβ (36). The Qβ complex is responsible for the replication of the single-stranded RNA genome of coliphage Qβ. Both EF-Tu and EF-Ts are components of the Qβ-polymerase complex along with the Qβ-replicase subunit and ribosomal protein S1 (37–39). The region that corresponds to the *T. thermophilus* coiled-coil region of one monomer is reduced in size in bovine EF-Ts$_{mt}$ and forms a β-strand, $\beta 2'$, in subdomain N. The coiled-coil region of the second EF-Ts moiety in the *T. thermophilus* EF-Tu·Ts complex, which is equivalent to the coiled-coil motif of *E. coli* EF-Ts, is reduced to a large loop packing against subdomain C of bovine EF-Ts$_{mt}$. The coiled-coil motif is conserved in bacteria and chloroplasts. It has been suggested that the coiled-coil motif of *E. coli* EF-Ts is involved in an isomerization step within EF-Ts during the formation of the EF-Tu·GDP·EF-Ts complex that acts as an intermediate in the nucleotide exchange reaction (35). This type of isomerization step has been studied with the nucleotide exchange reaction taking place with the ternary EF-Tu·thioGDP·EF-Ts complex (40). Furthermore, it has been suggested that the binary EF-Tu·Ts complex and the ternary complex with either GDP or GTP are structurally distinct (41). Clearly, the absence of the coiled-coil motif in EF-Ts$_{mt}$ suggests that any isomerization reaction occurring with the mitochon-

TABLE II
Interpretation of mutations in EF-Ts$_{mt}$ made previously

EF-Ts$_{mt}$ mutant[a]	Location	Effect on activity	Structural analysis	Ref.
R67A, R68A, K69A	Amino-terminal	No change	Hydrogen bonding here not important	34
K78A, K79A	Amino-terminal	No change	sLys^{79} too far away to make contact with EF-Tu$_{mt}$	34
F74A, I75A	Amino-terminal	Down 2-fold	Loss of hydrophobic interactions with helix D of EF-Tu$_{mt}$	34
F74M, I75M	Amino-terminal	No change	Met can replace the hydrophobic interactions of Phe and Ile	34
F74E, I75E	Amino-terminal	Inactive	Interaction of N-terminal domain of EF-Ts$_{mt}$ with domain I of EF-Tu$_{mt}$ is essential	34
D139A	Subdomain N	Down 5-fold	Loss of hydrogen bond interactions with helix B of EF-Tu$_{mt}$	33
F140A	Subdomain N	Down 5-fold	Loss of hydrophobic interactions with uTyr^{133} and uLeu^{167}. Can not disrupt orientation of helices B and C of EF-Tu$_{mt}$	33
D139A, F140A	Subdomain N	Inactive	The disruption of this region of EF-Tu$_{mt}$ is essential for release of guanine nucleotides	33
H231A	Subdomain C	Down 6-fold	Hydrogen bond of His side chain with domain III of EF-Tu$_{mt}$ is important in their interaction, and loss of this interaction decreases its ability to promote guanine nucleotide exchange	34
R267A, R268A	Subdomain C	No change	Hydrogen bond from sArg^{268} to EF-Tu$_{mt}$ not important for their interaction	34
L302V, L303M	Subdomain C	No change	Hydrophobic contacts maintained	34
L302E, V303E	Subdomain C	Down 7-fold	Disrupts binding due to loss of hydrophobic contacts with domain III	34

[a] Numbering refers to the precursor protein and is different from the numbering in the indicated reference, which refers to the mature protein.

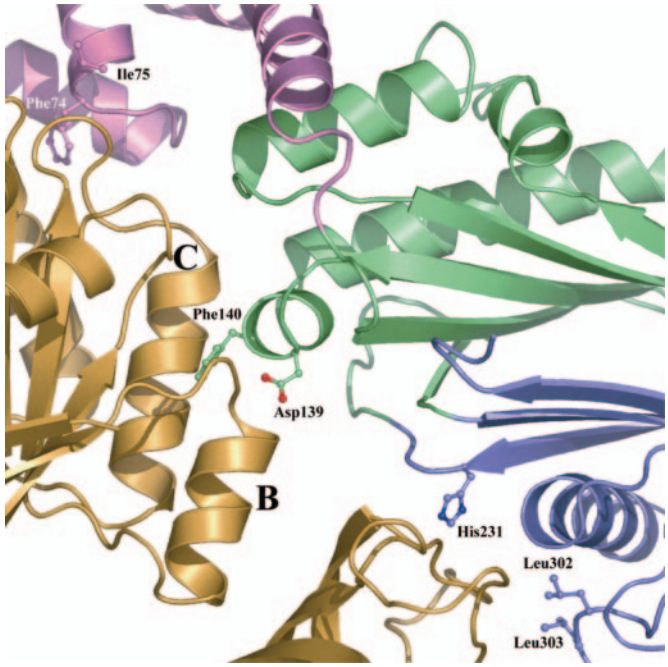

FIG. 6. **Position of previously mutated residues in the bovine EF-Tu$_{mt}$·Ts$_{mt}$ interface.** See Table II for an overview of mutations made in mitochondrial EF-Ts$_{mt}$. Some of the mutated residues of EF-Ts$_{mt}$ are shown in *stick representation* and labeled along with helices B and C from EF-Tu$_{mt}$. Coloring of the EF-Tu$_{mt}$·Ts$_{mt}$ complex is as described in Fig. 1*A*. See "Results" for discussion.

drial factor must involve other parts of the molecule.

The observation that the EF-Ts proteins have the highest sequence identity in the amino terminus obviously signifies the importance of this domain in the nucleotide exchange reaction. The fact that mutation of the aspartic acid and phenylalanine residues from the TDFV motif in *E. coli* and bovine mitochondrial EF-Ts yielded different results reflects the idea that the exchange reaction is a result of several effects mediated by EF-Ts, perhaps mainly by the amino terminus. The relative importance of each effect appears to vary with the factors from different translational systems.

The movement of part of the NKXD motif and the following loop could be a significant contribution to the exclusion of GDP from EF-Tu$_{mt}$, and other G-proteins in general. The Ran·RCC1 complex is suggested to release the base of the guanine first, followed by the phosphate moiety (28). This complex and that of Ras·Sos1 (27) both posses a NKXD motif that is structurally different from that seen in *E. coli* and *T. thermophilus* EF-Tu·Ts but somewhat similar to the one in the EF-Tu$_{mt}$·Ts$_{mt}$ complex. However, the weak density in this region of our structure does not convincingly suggest the specific mechanism at work. A higher mobility of the guanine binding region was suggested as the main reason for the low affinity of EF-Tu$_{mt}$ for nucleotides (10).

The interaction between EF-Ts$_{mt}$ and EF-Tu$_{mt}$·GDP leads to quite large conformational changes in EF-Tu$_{mt}$. These conformational changes involve a considerable shift in the interactions of the three domains of EF-Tu$_{mt}$. Of particular interest is the difference in the interface between domain II and III of EF-Tu$_{mt}$, as well as their relative position between the GDP and EF-Ts$_{mt}$ complexed forms. These differences have not been observed in the other EF-Tu·Ts complexes from *E. coli* and *T. thermophilus* (14, 15). Thus, in the bovine EF-Tu$_{mt}$·Ts$_{mt}$ complex, domains II and III do not act as a rigid body as observed in *E. coli* and *T. thermophilus* EF-Tu.

When superimposing the parts of EF-Ts that interact with EF-Tu along with EF-Tu helices B and C of domain I from *E. coli*, *T. thermophilus*, and *B. taurus*, there is a relatively large shift in the position of domain III of EF-Tu$_{mt}$ relative to domain III in the other complexes that are almost superimposed. The three complexes differ mainly in the distance between helix D of EF-Tu and helix α1 of EF-Ts. Helix α1 in EF-Ts$_{mt}$ is extended compared with the corresponding helices in the prokaryotic factors, and it lies closer to helix D than in either of the other two bacterial complexes. The implications of these differences must await further biochemical and structural studies.

Acknowledgment—We thank Santosh Panjikar at the DORIS storage ring (DESY) for technical assistance during data collection.

REFERENCES

1. Czworkowski, J., and Moore, P. B. (1996) *Prog. Nucleic Acid Res. Mol. Biol.* **54,** 293–332
2. Green, R., and Noller, H. F. (1997) *Annu. Rev. Biochem.* **66,** 679–716
3. Clark, B. F., and Nyborg, J. (1997) *Curr. Opin. Struct. Biol.* **7,** 110–116
4. Scheffler, I. E. (1999) *Mitochondria* Wiley-Liss, Inc., New York
5. Fox, T. D. (1987) *Annu. Rev. Genet.* **21,** 67–91
6. Helm, M., Brule, H., Friede, D., Giege, R., Putz, D., and Florentz, C. (2000) *RNA* (*N. Y.*) **6,** 1356–1379
7. O'Brien, T. W. (2002) *Gene* (*Amst.*) **286,** 73–79
8. Spremulli, L. L., Coursey, A., Navratil, T., and Hunter, S. E. (2004) *Prog. Nucleic Acid Res. Mol. Biol.* **77,** 211–261
9. Woriax, V. L., Burkhart, W., and Spremulli, L. L. (1995) *Biochim. Biophys. Acta* **1264,** 347–356
10. Andersen, G. R., Thirup, S., Spremulli, L. L., and Nyborg, J. (2000) *J. Mol. Biol.* **297,** 421–436

11. Polekhina, G., Thirup, S., Kjeldgaard, M., Nissen, P., Lippmann, C., and Nyborg, J. (1996) *Structure* (*Lond.*) **4,** 1141–1151
12. Song, H., Parsons, M. R., Rowsell, S., Leonard, G., and Phillips, S. E. (1999) *J. Mol. Biol.* **285,** 1245–1256
13. Xin, H., Woriax, V., Burkhart, W., and Spremulli, L. L. (1995) *J. Biol. Chem.* **270,** 17243–17249
14. Kawashima, T., Berthet-Colominas, C., Wulff, M., Cusack, S., and Leberman, R. (1996) *Nature* **379,** 511–518
15. Wang, Y., Jiang, Y., Meyering-Voss, M., Sprinzl, M., and Sigler, P. B. (1997) *Nat. Struct. Biol.* **4,** 650–656
16. Doublie, S. (1997) *Methods Enzymol.* **276,** 523–530
17. Bradford, M. M. (1976) *Anal. Biochem.* **72,** 248–254
18. Otwinowski, Z., and Minor, W. (1997) in *Macromolecular Crystallography, Part A, Methods in Enzymology Series, Vol. 276* (Carter, C. W., Jr., and Sweet, R. S., eds) pp. 307–326, Academic Press, New York
19. Brunger, A. T., Adams, P. D., Clore, G. M., DeLano, W. L., Gros, P., Grosse-Kunstleve, R. W., Jiang, J. S., Kuszewski, J., Nilges, M., Pannu, N. S., Read, R. J., Rice, L. M., Simonson, T., and Warren, G. L. (1998) *Acta Crystallogr. Sect. D Biol. Crystallogr.* **54,** Pt 5, 905–921
20. Jones, T. A., Zou, J. Y., Cowan, S. W., and Kjeldgaard. (1991) *Acta Crystallogr. Sect. A* **47,** Pt 2, 110–119
21. Laskowski, R. A., MacArthur, M. W., Moss, D. S., and Thornton, J. M. (1993) *J. Appl. Cryst.* **26,** 283–291
22. Kabsch, W., and Sander, C. (1983) *Biopolymers* **22,** 2577–2637
23. DeLano, W. L. (2002) *The PyMOL User's Manual*, DeLano Scientific, San Carlos, CA
24. Jiang, Y., Nock, S., Nesper, M., Sprinzl, M., and Sigler, P. B. (1996) *Biochemistry* **35,** 10269–10278
25. Deleted in proof
26. Sprang, S. R. (1997) *Annu. Rev. Biochem.* **66,** 639–678
27. Boriack-Sjodin, P. A., Margarit, S. M., Bar-Sagi, D., and Kuriyan, J. (1998) *Nature* **394,** 337–343
28. Renault, L., Kuhlmann, J., Henkel, A., and Wittinghofer, A. (2001) *Cell* **105,** 245–255
29. Berchtold, H., Reshetnikova, L., Reiser, C. O., Schirmer, N. K., Sprinzl, M., and Hilgenfeld, R. (1993) *Nature* **365,** 126–132
30. Kjeldgaard, M., Nissen, P., Thirup, S., and Nyborg, J. (1993) *Structure* (*Lond.*) **1,** 35–50
31. Andersen, G. R., Pedersen, L., Valente, L., Chatterjee, I., Kinzy, T. G., Kjeldgaard, M., and Nyborg, J. (2000) *Mol. Cell* **6,** 1261–1266
32. Zhang, Y., Yu, N. J., and Spremulli, L. L. (1998) *J. Biol. Chem.* **273,** 4556–4562
33. Zhang, Y., Li, X., and Spremulli, L. L. (1996) *FEBS Lett.* **391,** 330–332
34. Zhang, Y., and Spremulli, L. L. (1998) *J. Biol. Chem.* **273,** 28142–28148
35. Karring, H., Bjornsson, A., Thirup, S., Clark, B. F., and Knudsen, C. R. (2003) *Eur. J. Biochem.* **270,** 4294–4305
36. Karring, H., Mathu, S. G., van Duin, J., Clark, B. F., Kraal, B., and Knudsen, C. R. (2004) *J. Biol. Chem.* **279,** 1878–1884
37. Kamen, R. (1970) *Nature* **228,** 527–533
38. Blumenthal, T., Landers, T. A., and Weber, K. (1972) *Proc. Natl. Acad. Sci. U. S. A.* **69,** 1313–1317
39. Wahba, A. J., Miller, M. J., Niveleau, A., Landers, T. A., Carmichael, G. G., Weber, K., Hawley, D. A., and Slobin, L. I. (1974) *J. Biol. Chem.* **249,** 3314–3316
40. Eccleston, J. F., Kanagasabai, T. F., and Geeves, M. A. (1988) *J. Biol. Chem.* **263,** 4668–4672
41. Gromadski, K. B., Wieden, H. J., and Rodnina, M. V. (2002) *Biochemistry* **41,** 162–169